Revision_2

A single-crystal neutron diffraction study of berborite 2*T*, $Be_2(BO_3)(OH)\cdot H_2O$

G. Diego Gatta, Nicola Rotiroti, Geoffrey Bromiley, Jan C.M. de Hoog, Jörgen Langhof and Oscar Fabelo

Running title: Crystal chemistry of berborite reinvestigated

Corresponding author: G. Diego GATTA
Dipartimento di Scienze della Terra, Università degli Studi di Milano
Via Botticelli 23, I-20133 Milano, Italy
Tel. +39 02 503 15607, E-Mail: diego.gatta@unimi.it

Manuscript submitted to American Mineralogist

This is the peer-reviewed, final accepted version for American Mineralogist, published by the Mineralogical Society of America.
The published version is subject to change. Cite as Authors (Year) Title. American Mineralogist, in press.
DOI: https://doi.org/10.2138/am-2025-10029. http://www.minsocam.org/

A single-crystal neutron diffraction study of berborite 2*T*, $Be_2(BO_3)(OH)\cdot H_2O$

G. Diego Gatta[1], Nicola Rotiroti[1], Geoffrey Bromiley[2], Jan C.M. de Hoog[2], Jörgen Langhof[3] and Oscar Fabelo[4]

[1]Dipartimento di Scienze della Terra, Università degli Studi di Milano,
Via Botticelli 23, I-20133 Milano, Italy
[2] School of Geosciences, The University of Edinburgh, UK
[3] Department of Geosciences, Swedish Museum of Natural History, SE-104 05, Stockholm, Sweden
[4]Institut Laue-Langevin, 71 Avenue des Martyrs, F-38000 Grenoble, France

Abstract

The chemical composition (by EPMA-WDS and SIMS) and the crystal structure (by single-crystal X-ray diffraction at 293 K and neutron diffraction at 20 K) of berborite-2*T* from the Saga II quarry at Auenlandet, Larvik plutonic complex in southern Norway, were investigated. Chemical and crystallographic data confirm the general mineral formula of berborite: $Be_2(BO_3)(OH)\cdot H_2O$. F and Cl content (as potential substituents of the OH-group) was found to be below the detection limit of EPMA-WDS, and the average content of the other measured elements (*i.e.,* Na, K, Ca, Mg, Fe, and S) is lower than 600 wt. ppm per equivalent oxide, and probably ascribable to micro-inclusions of other mineral species, rather than to elements replacing B or Be in berborite structure. Excluding B and Be, both considered as "critical elements" for the modern technology, berborite does not contain other industrially-relevant elements. The measured $^{11}B/^{9}Be$ ratio of berborite by SIMS was consistent with the expected value of the ideal formula (*i.e.,* 1B : 2Be a.p.f.u).

X-ray and neutron refinements confirm the previously reported general structural model of berborite-2*T*, built up by two layers made by regular (as governed by the 3-fold axes) corner-sharing triangular BO_3-units and tetrahedral $BeO_3\Phi$ (Φ = OH, H_2O) units, mutually connected to give electron-neutral $[(BO_3)Be_2\Phi_2]$-layers. The Φ-groups (*i.e.,* hydroxyls or H_2O molecules) represent the out-of-plane apices of the tetrahedra, and the special position of the O sites on the triad implies a statistical occupancy of the Φ-groups (*i.e.*, 1/3 OH and 2/3 H_2O). Subsequent electron-neutral $[(BO_3)Be_2\Phi_2]$-layers are mutually connected only by H-bonds. The statistical occupancy of the H sites leads to a complex configuration of the H-bonding network, here described on the basis of the neutron diffraction data. The calculation of the difference-Fourier maps of the nuclear density function and the application of the Maximum Entropy Method to the experimental data consistently rule out dynamic disorder of the H sites, confirming the occurrence of a static disorder of the protons in the structure of berborite-2*T*, at least at 20 K.

Keywords: Berborite, crystal chemistry, EPMA-WDS, SIMS, X-ray and neutron diffraction, hydrogen bonding.

Introduction

Berborite is an uncommon mineral, and one of the few containing both B and Be as major components (from which its name is derived: BERyllium and BORate). It had been found in a few localities worldwide, the two most important being: Lupikko mine, Pitkyaranta mining district, Republic of Karelia, Russia, where berborite occurs in serpentinized dolostone associated with W–Sr–B–Be-bearing skarns, usually associated with hambergite, schoenfliesite, helvite, apatite, cassiterite, fluorite, calcite, dolomite, magnetite (and other minerals) (Nefedov 1967; Nefedov et al. 1977 and references therein); Saga quarries, Sagåsen, Porsgrunn, Telemark and several quarries in the Tvedalen area, Larvik, Vestfold, Norway, in which berborite occurs in vugs with natrolite and thomsonite in nepheline-syenite pegmatites (Larsen 2010, and references therein). Lupikko Mine is the type locality of the mineral. Crystals of berborite are usually colorless and nearly transparent; it is found in rare cases as individual crystals up to 5 mm in size, although is more often found in intergrown groups. The habit of berborite crystals differs in response to the different symmetry of the crystal structure (crystal systems: trigonal, hexagonal), as three different polytypes are known (details will be given below): hexagonal prism {100}, steep hexagonal pyramids {201}, {101} and {113}, trigonal pyramids or trigonal prisms, and hexagonal pyramid modified with a trigonal pyramid.

Berborite was described as a new mineral species by Nefedov (1967) (see also Fleischer 1968; Nikolskaia and Larin 1972; Nefedov et al. 1977). Chemical characterization by spectrographic analysis, loss of ignition and thermal analysis, along with unit-cell parameters derived by X-ray diffraction and calculated density, yield the following ideal formula: $Be_2(BO_3)(OH,F)\cdot H_2O$ (F *ca.* 1.0-1.5 wt%). DTA showed an endothermic reaction at 200-340 °C and another at 680-830°C, followed by an exothermic reaction at 850-950 °C, with a total loss of weight of *ca.* 24% (see Fig. 2 in Nefedov 1967). X-ray Laue photographs showed symmetry-class -3*m*, with unit-cell parameters: a~4.43 and c~ 5.53 Å.

Schlatti (1967, 1968) solved the crystal structure of the synthetic counterpart of berborite by powder X-ray diffraction data. The diffraction pattern was indexed with unit-cell parameters a~4.43 and c~5.34 Å, and the structure was described in the space group *P*321. The structural model of Schlatti (1967, 1968) left a series of open questions about a disordered configuration of the hydroxyl groups and H_2O molecules within the crystalline edifice. Later, a reinvestigation of the crystal structure of berborite was performed by Giuseppetti et al. (1990). In their seminal paper, the authors

showed how at least three different polytypes of berborite occur in nature: berborite-1*T* (*a*~4.434 and *c*~5.334 Å, space group *P*3), berborite-2*T* (*a*~4.431 and *c*~10.663 Å, space group *P*3*c*1), and berborite-2*H* (*a*~4.433 and *c*~10.638 Å, space group $P6_3$). X-ray diffraction data were collected on a 4-circle diffractometer equipped with a point-detector. Crystals of the three polytypes came from the same locality: nepheline-syenite pegmatite of the Saga larvikite quarry, Tvedalen district, Norway, with the different polytypes exhibiting different crystal morphologies. Giuseppetti et al. (1990) also reported some physical and optical properties of the berborites under investigation, along with the chemical composition as derived by electron probe microanalysis in wavelength-dispersive mode and additional wet analyses by atomic absorption spectrometry and ion chromatography. The combination of chemical and crystallographic data confirmed the ideal formula of berborite previously reported: $Be_2(BO_3)(OH)\cdot H_2O$ (F content not relevant). The structural model of the berborite-1*T* should be virtually identical to that reported by Schlatti (1967, 1968). However, the model of Giuseppetti et al. (1990) is similar but not identical to the previous one, with minor differences ascribable to the OH- and the H_2O-sites, which are not equivalent as modelled in Schlatti (1967, 1968). The berborite-1*T* structure contains a single layer made by regular (as governed by the 3-fold axes) corner-sharing triangular BO_3-units and tetrahedral $BeO_3\Phi$ (Φ = OH, H_2O) units, mutually connected to give an electron-neutral $[(BO_3)Be_2\Phi_2)]$-layer. The triangular bases of tetrahedral $BeO_3\Phi$-units lie on the same plane as the BO_3-units, but 50% point to one direction (+*c*) and 50% in the opposite direction (-*c*). The Φ-groups represent the out-of-plane apices of the tetrahedra. Due to statistical occupancy of the Φ-groups, a complex configuration of hydrogen bonds occurs in the structure of berborite. According to Giuseppetti et al. (1990), the real symmetry of berborite-1*T* is *P*3, despite the crystalline edifice showing a pseudo-symmetry *P*321. The two additional polytypes discovered by Giuseppetti et al. (1990) show a doubling of the unit-cell edge length along [0001] and, therefore, two electron-neutral $[(BO_3)Be_2\Phi_2]$-layers in the unit-cell, along with stacking of the layers compared to the 1*T* polytype (*e.g.*, berborite-2*T* could be derived from the 1*T* by a 180° rotation about the triad of all the triangular and tetrahedral units in alternate layers). Fig. 6 from Giuseppetti et al. (1990) illustrates differences in the structures of the three different polytypes. The causes of polytypism in berborite were not fully determined by Giuseppetti et al. (1990), but it was presumed that the polytypism is somehow governed by disorder of the OH *vs.* H_2O groups, and subsequent differences in H-bonding schemes within the structure. However, the elusive nature of H for X-ray diffraction made it difficult to provide a clear picture of the role played by protons, especially considering their partial site occupancy (1/3 or 2/3, according to Giuseppetti et al. 1990) within the structure of berborite.

Very recently, an additional study on the local state of hydrogen atoms in the crystal structure of natural berborite (polytype 1*T*, modelled in the space group *P*321) was performed by Aksenov et al. (2024), on the basis of *in-situ* low-temperature single-crystal X-ray analysis (between 293 and 90 K), and IR and ^{1}H NMR spectroscopy. The experimental data shows that in the structure of berborite-1*T* there are two independent systems of hydrogen bonds involving mobile protons (by partial proton transfer mechanisms from donor to acceptor of H-bonds, due to similar O_D-H and H…O_A distances in a O_D-H…O_A bond). The presence of additional isolated H^+ protons in the interlayer space was also presumed. *In-situ* low-*T* data showed evidence of a complete stabilization of protons at a critical "freezing-point" of 243 K. However, the authors were unable, based on X-ray analysis, to locate the position of these extra protons; instead, neutron diffraction is required.

In this light, the aim of this study is a reinvestigation of the crystal structure and chemical composition of natural berborite from the Saga II quarry at Mörje, Larvik plutonic complex in southern Norway, on the basis of a multi-methodological approach, based on single-crystal X-ray (at room temperature) and neutron diffraction (at low temperature), electron probe microanalysis in wavelength-dispersive mode (EPMA-WDS) and Secondary Ion Mass Spectrometry (SIMS), in order to provide: *i*) a full chemical characterization of this mineral, with major, minor and trace elements, *ii*) a structural model, based on neutron diffraction data, with an unambiguous location and description of anisotropic displacement regime of all the proton sites, coupled with the H-bonding configuration in the structure of berborite. The paucity of the sample did not allow additional investigation based, for example, on thermo-gravimetric analysis. This manuscript follows a series of studies performed on hydrous B- and Be-bearing minerals, including hambergite [$Be_2BO_3(OH,F)$, Gatta et al. 2012], epididymite and eudidymite ($Na_2Be_2Si_6O_{15}\cdot H_2O$ Gatta et al. 2008) and inderborite [$CaMg[B_3O_3(OH)_5]_2(H_2O)_4\cdot 2H_2O$, Gatta et al. 2024].

Sample description and occurrence

Crystals of berborite used for this multi-methodological study were taken up from specimen #NRM19850008, Swedish Museum of Natural History, Stockholm, Sweden. The berborite crystal aggregate originates from the Saga II quarry at Auenlandet, at the Larvik plutonic complex in southern Norway, which hosts the best finds of berborite in the world. About ten different alkaline pegmatites have been found to contain berborite. At the Saga II quarry, berborite occurs in vugs filled by natrolite (the so-called "*Spreustein*"), hydrothermally altered nepheline, along with böhmite, behoite and calcite (Larsen 2010).

Experimental methods and Results

Chemical characterization

The concentration of minor and trace elements in two berborite crystals (*ca.* 100 x 150 x 300 μm) was measured by EPMA-WDS, using a JEOL 8200 Super Probe system at the COSPECT facility, University of Milan, with operating conditions: 15 kV and 5 nA, 10 μm beam diameter, 30 s of counting times on the peaks and 10 s on the backgrounds. The two crystals were mounted in epoxy resin (in a round sample mount, ∅ 1.0 inch), polished and then coated with a thin film of electrically-conductive carbon. Natural compounds were used as standards and data corrected for matrix effects using a *ZAF* routine implemented in the JEOL suite of programs. The following standards were used: K-feldspar (K), omphacite (Na), forsterite (Mg), fayalite (Fe), grossular (Al, Si, Ca), marialite (Cl), celestine (S), and apatite (F). The two analysed crystals were found to be chemically homogeneous. Only Na, K, Mg, Ca, Fe, and S were measured at a significant level; F and Cl were not detected. However, a modest degradation of the crystals was observed under the electron beam, even after increasing beam diameter from 10 up to 20 μm. The EPMA-WDS data are listed in Table 1.

A crystal from the same berborite sample was also investigated by Secondary Ion Mass Spectrometry (SIMS) using a Cameca ims 7f-GEO at the University of Edinburgh Ion Microprobe Facility to determine the Be and B content. A primary ion beam consisting of $16O^-$ and a beam current of 5 nA was accelerated to 13 kV and impacted upon a polished section of the sample, mounted in epoxy. The sample was gold-coated prior to analysis to avoid charging effects, and kept under ultrahigh vacuum (*ca.* $2x10^{-8}$ mbar) during analysis. The analytical spot size was *ca.* 10 μm in diameter. Secondary ions sputtered from the sample surface were filtered based upon their energy, only allowing positive ions with an energy range of 75 ± 25 eV to pass into the mass spectrometer, and were counted using an electron multiplier. A mass resolution of 2000 (M/ΔM) was used to avoid interference of $^9BeH_2^+$ with $^{11}B^+$, $^9Be^{10}B^+$ with $^{19}F^+$, $^{11}B^{16}O^+$ with $^{27}Al^+$, and $^{17}O^{18}O^+$ with ^{35}Cl he following isotopes were measured sequentially during 8 cycles of the magnet, with total measuring time in brackets: ^1H (24s), ^7Li (24s), ^9Be (8s), ^{11}B (8s), ^{19}F (40s), ^{27}Al (16s), ^{28}Si (16) and ^{35}Cl (40). Peak positions were determined using NIST SRM610 glass. Hambergite #102984 (Dyar et al. 2001) was used as a calibration standard for Be and B. We also measured an in-house gem quality, stoichiometric fluorite crystal (Blue John mine) to estimate the ^{19}F yield, as no F is reported for hambergite #102984. The SIMS data are listed in Table 2.

The measured $^{11}B/^9Be$ ratio of berborite by SIMS was indistinguishable from that of the hambergite standard (Table 2), whereas $^1H/^9Be$ was 1.9 times higher. ^9Be count rates were similar for

both minerals. Repeat analyses demonstrate that the crystal is homogeneous, with <1% rsd for ^{1}H, ^{11}B and ^{9}Be for 6 analytical spots. Only trace amounts of Li, F, Al, Si and Cl were detected. SIMS is a comparative technique that typically uses the known concentration of an abundant matrix element for quantification. This was not possible in this case, as the main elements present in berborite are challenging to accurately measure by electron beam techniques. Alternatively, quantification is possibly by measuring all elements and normalizing to 100% (as oxides). All major elements from EMPA-WDS data were present in concentrations <0.15 wt% and totalled <0.2 wt% (Table 1). Other elements such as F, Cl and Si were present at low levels (see below). Thus, we normalised the three main elements to 99.5 wt.% using ion yields of ^{1}H and ^{11}B relative to ^{9}Be in hambergite #102984 for calibration, using a stoichiometric hambergite #102984 composition of 8.93 H_2O, 37.09 B_2O_3 and 53.31 wt% BeO. These values differ slightly from the measured values in Dyar et al. (2001), but those were associated with large uncertainties and totalled 97.7 wt%, even though hambergite #102984 was shown to be almost pure Be_2BO_3OH. Low levels of other elements are supported by our own hambergite #102984 measurements. Based on this approach, we determined the berborite composition as 33.9 B_2O_3, 48.8 BeO and 16.8 wt% H_2O, resulting in a mineral formula of $Be_2BO_3OH(H_2O)_{0.46}$. Concentrations of other elements were estimated using empirical relative ion yields, based on NIST610, resulting in ca. 0.01 µg/g Li, 120 µg/g F, 3 µg/g Al, 3250 µg/g Si (= 0.7 wt. % SiO_2) and 0.5 µg/g Cl.

Single-crystal X-ray and neutron diffraction

- ***X-ray and neutron data collections and treatments***

Two crystals of berborite, observed as free of defects and inclusions by optical microscopy, were selected for single-crystal X-ray (size: 0.08 × 0.12 × 0.18 mm) and neutron (size: 2.2 x 2.2 x 3.1 mm) diffraction experiments. The quality of the crystals was first assessed using a KUMA-KM4 four-circle X-ray diffractometer (available at the COSPECT facility, University of Milan).

The X-ray intensity data collection of berborite was performed at room temperature (293(1) K) with a Rigaku XtaLABSynergy-i X-ray diffractometer, equipped with a PhotonJet-i Mo*K*α microfocus source and a HyPix-6000HE HPC detector, at the Earth Sciences Department, University of Milan. Diffraction data were collected using an ω-scan strategy, with 0.5° step size and an exposure time of 1 s/frame, with an *ad hoc* routine (optimised by the *CrysAlisPro* suite; Rigaku-Oxford Diffraction 2019) aimed to maximize the reciprocal space coverage. A total number of 14472 Bragg reflections were collected up to $2\theta_{max}$ of 74.66° (with $d_{min} \sim 0.58$ Å and $-7 \leq h \leq +7$, $-7 \leq k \leq +7$ and

This is the peer-reviewed, final accepted version for American Mineralogist, published by the Mineralogical Society of America.
The published version is subject to change. Cite as Authors (Year) Title. American Mineralogist, in press.
DOI: https://doi.org/10.2138/am-2025-10029. http://www.minsocam.org/

$-18 \leq l \leq +17$). The diffraction pattern was successfully indexed with a metrically trigonal unit-cell, with $a = 4.4319(1)$ Å and $c = 10.6636(2)$ Å, giving 628 reflections unique for symmetry ($R_{int} = 0.0332$, Laue class $\bar{3}m$) and 625 with $F_o > 4\sigma(F_o)$. The reflection conditions were consistent with the space group $P3c1$. Unit-cell parameters and symmetry were those expected for the berborite-2*T* polytype of Giuseppetti et al. (1990). Integrated intensity data were then corrected for the effects of Lorentz-polarization and for X-ray absorption effects using the *ABSPACK* routine (with a semi-empirical strategy) of the *CrysAlisPro* package (Rigaku-Oxford Diffraction 2019). The Wilson plot and the distribution statistics of the normalized structure factors suggested that the structure of the berborite under investigation is acentric (at 60% likelihood). Twinning by merohedry was found to affect the crystal (twin law: 010, 100, 00$\bar{1}$; two domains with fractional contribution: 50%). Additional details of the X-ray data collection and treatment are given in Table 3 (*deposited*) and in the CIF (*deposited*).

The morphology of the crystal of berborite, selected for the neutron diffraction experiment, can be described by a large pedion and a ditrigonal pyramid modified by a trigonal pyramid, very similar to that of the crystal of berborite-2*T* used by Giuseppetti et al. (1990) and shown in Fig. 3 of their manuscript. For the neutron diffraction experiment, the crystal was mounted on an Al pin and placed on a close-circuit displex device four-circle D9 diffractometer at the Institute Laue-Langevin, Grenoble, France. Monochromatic radiation with a constant wavelength of 0.835 Å (as obtained from a Cu(220) monochromator) was used for the diffraction experiment, and low-temperature data were collected at 20(1) K (Archer and Lehmann 1986). The D9 diffractometer was equipped with a small two-dimensional area detector. The data collection strategy consisted of a series of ω-scans (for low-Q reflections) and ω-2θ scans (for high-Q reflections), varying the ω-range in response to the instrument resolution curve. 2130 Bragg reflections were collected up to $2\theta_{max}$ of 116.87° (with d_{min} ~ 0.50 Å, in the range $-8 \leq h \leq +8$, $-9 \leq k \leq +8$ and $-19 \leq l \leq +3$), out of which 356 refls. were unique for symmetry ($R_{int} = 0.0320$, Laue class $\bar{3}m$) and 350 with $F_o > 4\sigma(F_o)$. Integrated intensities were first corrected by background and for Lorentz effects, adopting the *Racer* program (Wilkinson et al. 1988), and then by absorption, based on shape and chemical composition of the crystal, using the ILL program *Datap* (available in the online *SXtalSoft* repository, https://code.ill.fr/scientific-software/sxtalsoft). The diffraction pattern was successfully indexed with a metrically trigonal unit-cell, with $a = 4.4389(7)$ Å and $c = 10.662(1)$ Å, and the reflection conditions were consistent with the space group $P3c1$, according to experimental findings based on the X-ray data. The Wilson plot and the distribution statistics of the normalized structure factors suggested that the structure is acentric (at ~76% likelihood). Evidence of twinning by merohedry were observed, but not significant (twin law:

010, 100, 00$\bar{1}$; two domains with fractional contribution: 99.0(3)% and 1.0(3)%). Further details pertaining to neutron data collection are given in Table 3 (*deposited*) and in the CIF (*deposited*).

- ***X-ray and neutron structure refinements***

X-ray and neutron structure refinements were performed using the SHELXL-2018/3 software (Sheldrick 2015) in the space group *P*3*c*1, starting from the structure model of berborite-2*T* reported by Giuseppetti et al. (1990), without any H site.

For the X-ray structure refinement (data collected at 293 K), the atomic form factors for B, Be, O and H were taken from the *International Tables for Crystallography Vol. C*. Secondary isotropic extinction effects were modelled and corrected according to Larson formalism (1967). Convergence was rapidly achieved after the first cycles of isotropic refinement. Further cycles were then conducted with the atomic sites modelled anisotropically. When convergence was achieved, two independent H sites, *i.e.*, *H*1 and *H*2 (Table 4, *deposited*), where added to the structure model: their atomic coordinates were deduced by inspection of the difference-Fourier maps of the electron density function, and modelled as isotropic (restraining the two sites to share the same isotropic displacement parameter). With such a model, convergence was rapidly achieved and the variance-covariance matrix showed no significant correlation among the refined parameters. At the end of the refinement, all the principal mean-square atomic displacement parameters were positive, and the intensity of the most significant residual peaks, in the difference-Fourier map of the electron density function, were $< \pm 0.4$ *e*-/Å^3. The final $R_1(F)$, according to the SHELXL-2018/3 definition, was 0.0264, for 625 observed refls. and 33 refined parameters. Further details pertaining to the X-ray structure refinement are listed in Table 3 (*deposited*). The atomic coordinates and displacement parameters (coupled with the principal root-mean-square components) are listed in Tables 4, 5 and 6 (*all deposited*) and in the CIF (*deposited*). Some selected structural parameters (interatomic distances and angles) are given in Table 7.

For the neutron structure refinement (data collected at 20 K), the H-free starting model was that previously refined by X-ray data. Neutron scattering lengths of B, Be, O and H were taken from Sears (1986). The effect of secondary extinction was modelled and corrected according to the formalism of Larson (1967), as implemented in SHELX, and the correction was found to be significant (*i.e.*, EXTI: 0.40(4); Table 3, *deposited*). After the first cycles of isotropic refinement, convergence was rapidly achieved with: *i*) two independent minima in the difference-Fourier map of the nuclear density function, at a distance from *O2A* and *O2B* sites consistent with O-H groups, and *ii*) one maximum lying on (0001) at the center of inertia of the "empty" triangle described by the three

O1s-*O1s*-*O1s* sites (Table 4, *deposited*; CIF). Two mutually-exclusive H sites, *i.e.*, *H1* and *H2* (Table 4, *deposited*) were then added to the structure model to account for the minima as residual peaks (as H has a negative neutron scattering length); the best figure of merit was obtained with *s.o.f.*(*H1*)=1/3 and *s.o.f.*(*H2*)=2/3. Fig. 2 shows the (0001) section of the difference-Fourier map of the nuclear density function at z=1/2, phased without any H sites in the structural model; the symmetry-related positions of the *H1* and *H2* sites are clearly visible as minima of the map, with higher nuclear density for the site ascribed to the *H2*. An additional site, modelled as partially populated by oxygen (*s.o.f.* ~13%, Table 4, *deposited*) and here labelled as *O1*, was also added to account for the maximum as residual peak of the difference-Fourier map. As shown in Fig. 1, the presence of the *O1* site can be ascribed to a local disorder generated by a 60° rotation of the Be-tetrahedra (or, consequently, of the BO_3-units), with a potential configuration of the polyhedra on (0001), as predicted by Giuseppetti et al. (1990). *O1* and *O1s* sites are, therefore, mutually exclusive, consistent with the refined *s.o.f.* (*i.e.,* ~13%*O1* and ~87%*O1s*; Table 4, *deposited*). We also verified if this disorder is not, alternatively, an overlooked result of twinning. The next cycles of refinement were then conducted with all atomic sites modelled as anisotropic. When convergence was achieved, no significant correlation, among the refined parameters, was observed in the variance-covariance matrix; all the principal mean-square atomic displacement parameters were positive. The final residuals in the difference-Fourier map of the nuclear density function were ≤ ±1.5 fm/Å^3. The final $R_1(F)$ was 0.0358, obtained for 350 observed refls. and 43 refined parameters. The refined structural model led to the chemical formula: $Be_2(BO_3)(OH)\cdot H_2O$. Additional details of the neutron refinement are reported in Table 3 (*deposited*). Atomic coordinates and displacement parameters are listed in Tables 4, 5 and 6 (*all deposited*) and in the CIF (*deposited*). Some selected structural parameters are given in Table 7.

An additional study, based on the Maximum Entropy Method (MEM), was performed in order to assess if the nature of the local disorder at the *H1* and *H2* sites, as derived by the neutron structure refinement, is static or dynamic. The MEM analysis is based on the principle of maximum entropy, which assumes that the most probable electron (or nuclear) density distribution is the one with the highest information entropy, consistent with the observed structure factor amplitudes *F*o and their standard uncertainties σ(*F*o) (Collins 1982). This approach does not rely on a predefined structural model and avoids model bias, making it particularly useful for identifying light elements, disorder, or diffuse features that may not be well captured by conventional Fourier maps. Entropy is maximized under the constraint that the calculated structure factors match experimental ones, within experimental uncertainty, providing a reconstructed density map compatible with the experimental data. For berborite, the analysis was carried out using the *Dysnomia* program (Momma et al. 2013),

which implements MEM in conjunction with structure factor data obtained from least-square single-crystal neutron diffraction refinement. The resulting maximum entropy maps we obtained showed positive density around the positions of B, Be, and O atoms, while negative density was observed near the expected H positions. The locations of these maxima (or minima for H atoms) were consistent with the proposed structural model based on neutron data. Although no structural model was provided during the MEM procedure, the final map revealed static disorder on (0001), affecting the configuration of the BO_3 units and/or the triangular basis of the Be-tetrahedra, with two distinguishable configurations clearly resolved. The density distribution indicated an unequal occupancy of the *O1* and *O1s* sites, in agreement with the refined values by the neutron structural refinement (*i.e.*, ~13% for *O1* and 87% for *O1s*; Table 4, *deposited*). Overall, the nuclear density was notably anisotropic, with the region around the B atom appearing the most spherical distribution. A slight contrast was also observed between the density profiles associated with the two independent Be sites, indicating a different Debye–Waller behaviour, which could potentially be ascribed to a partial substitution by other elements, although not detected by the chemical analysis of berborite (Tables 1 and 2), or to a different bonding configuration, which reflects the different Be-O-OH and Be-O-OH_2 bonds (*i.e.*, *BeA-O2A-H1 vs. BeB-O2B*-2(*H2*); Table 7, Fig. 1). The most intense negative density corresponded to the crystallographic position of the hydrogen atoms. As it will be discussed in the following section, the neutron structure refinement showed that each O-H group is disordered due to the presence of a 3-fold axis passing through the oxygen atom, which results in the hydrogen atom being distributed over three symmetry-equivalent positions. This feature was also clearly confirmed in the MEM map. Although the density was slightly displaced from the position obtained *via* neutron least-squares refinement, there was no indication of a ring-shaped distribution around the oxygen site, as shown in Fig. 3, which ruled out a dynamic disorder of the H sites.

Discussion and implications

Crystallographic, EPMA-WDS and SIMS (at least for B and Be) data of berborite from the Saga II quarry, obtained in this study, confirm the general chemical formula of the mineral previously reported in the literature: $Be_2(BO_3)(OH)\cdot H_2O$ (Nefedov 1967, Fleischer 1968, Giuseppetti et al. 1990). The fraction of F measured in this study, reported to be low but significant (*i.e.*, *ca.* 1.0-1.5 wt%) in samples from the Saga I quarry (Norway) and from the Luppikko deposit (Russia) (Nefedov 1967, Fleischer 1968, Giuseppetti et al. 1990), is below the detection limit of the EPMA-WDS (Table 1) and approximately 120 µg/g according to our SIMS measurements. The concentration of Cl, which along with F can also replace hydroxyl groups in many minerals, was found to be insignificant (Table

1). The average content of the other elements measured by EPMA (here reported as Na_2O, K_2O, CaO, MgO, FeO, and SO_3 in Table 1), is lower than 600 wt. ppm per each equivalent oxide. In contrast, SiO_2 is present at low levels (0.4-0.9 wt%) according our SIMS measurements, but was not detected by EPMA. We are inclined to believe that these elements are likely ascribable to micro-inclusions of different mineral species, rather than to elements replacing B or Be in the berborite structure. This is valid even for Si: it could replace Be in a framework of tetrahedra (as is noted in some zeolites or feldspars), though with a local chemical strain. However, in the structure of berborite, Si should be involved in a silanol group (*i.e.*, Si-O-H; giving tetrahedral SiO_3OH), a configuration only rarely observed in some open-framework materials (*e.g.*, zeolites). We also exclude the possibility that it can form $SiO_3(OH_2)$-groups with H_2O molecules. Excluding B and Be, both considered as "critical elements" for the modern technology, berborite does not contain other industrially-relevant elements.

SIMS data for the berborite crystal analysed imply a mineral formula: $Be_2BO_3OH(H_2O)_{0.46}$. B and Be content is consistent with the ideal chemical formula of the mineral, but the measured total H_2O fraction (*i.e.*, 16.8 wt%) is significantly lower than expected (*i.e.*, 24.6 wt%, for 1 OH group and 1 H_2O molecule p.f.u.), such that the number of molecules per formula unit is approximately half of the expected value. Due to an absence of suitable matrix-matched standards, Be, B and H concentrations were derived based on normalised ion yields compared to a stoichiometric hambergite standard. Although the Be/B ratios in stoichiometric hambergite and berborite are identical, H/Be ratios differ considerably. As such, inaccuracies in determined berborite H content may indicate a matrix effect, and underestimation in true H content in the H-rich berborite. However, although matrix effects for SIMS analysis remain difficult to predict, and there are differences in both H content and H bonding environment between hambergite and berborite, a matrix effect of sufficient magnitude to explain low determined H contents is unusual. DTA analysis of berborite indicates onset of H loss at temperatures as low as 200 °C (Nefedov 1967). However, impact by the primary ion beam during SIMS analysis does not typically result in sample heating and H loss, as beam power is very low. Alternatively, an H deficit during SIMS analysis could be ascribed to the fact that berborite is sensitive to high vacuum conditions used during the SIMS measurement, which could lead to a modest degradation (by dehydration) of the sample, even though repeat analyses gave consistent, low H contents. In contrast, refinement of neutron diffraction data here, and previous analysis of berborite by IR and ^{1}H NMR spectroscopy (Aksenov et al. 2024) and DTA (Nefedov 1967), confirm the stoichiometric H content of natural samples, and provide no evidence for variable H contents.

The crystal structure of berborite-2*T* obtained in this study confirms the general structural model previously reported by Giuseppetti et al. (1990): the structure is built up by two layers made

by regular (as governed by the 3-fold axes) corner-sharing triangular BO_3-units and tetrahedral $BeO_3\Phi$ (Φ = OH, H_2O) units, mutually connected to give electron-neutral $[(BO_3)Be_2\Phi_2]$-layers. Fig. 1 shows how the tetrahedral $BeO_3\Phi$-units have triangular bases lying on the same plane as BO_3-units, with 50% of tetrahedra pointing in one direction (+*c*) and 50% in the opposite direction (-*c*). The Φ-groups (*i.e.,* hydroxyls or H_2O molecules) represent the out-of-plane apices of these tetrahedra, and the special position of the O sites on the triad (*i.e., O2A* and *O2B*; Table 4) implies a statistical occupancy of the Φ-groups (*i.e.*, 1/3 OH and 2/3 H_2O; Table 4). Subsequent electron-neutral $[(BO_3)Be_2\Phi_2]$-layers are mutually connected only by hydrogen bonds, which, in turn, generate the perfect {0001} cleavage of crystals of berborite. The statistical occupancy of the H sites leads to a complex configuration of the H-bonding network. Fig. 4 shows one potential scenario of the H-bonding scheme in berborite, as dictated by the disordered configuration of the H sites, based on the neutron structure refinement from this study (data collected at 20 K). More specifically: *i*) the H-bonds occur between one OH-group and one H_2O molecule, never between pairs of hydroxyls or pairs of molecules, and *ii*) each *O2B* site (*i.e.*, of a H_2O molecule) is *donor* of two and *acceptor* of one H-bonds, whereas each *O2A* site (*i.e.*, of a OH-group) is *donor* of one and *acceptor* of two H-bonds. Some differences in the geometry of the H-bonding scheme occur in response to the different nature of OH^- *vs.* H_2O molecules: for the hydroxyl group, the *O2A-H1* distance (corrected for *riding motion* effect, Busing and Levy 1964) is ~0.998 Å, *O2A*…*O2B* is ~2.735 Å, *H1*…*O2B* is ~1.801 Å and the *O2A-H1*…*O2B* is ~175.6°; for the H_2O molecule, the *O2B-H2* (corrected for *riding motion* effect) is ~1.113 Å and *H2-O2B-H2* is ~105.6°, *O2B*…*O2A* is ~2.735 Å, *H2*…*O2A* is ~1.670 Å, and *O2B-H2*…*O2A* ~175.7°. The H-bonds are rather strong, and the geometry of the H_2O molecule is still in the range of the observed H-O-H angles in solid-state materials (*e.g.*, Chiari and Ferraris 1982; Steiner 1998; Gatta et al. 2008, 2021).

The neutron structural refinement of this study, with the calculation of the difference-Fourier maps of the nuclear density function, and the additional MEM calculation, which does not rely on a predefined structural model (avoiding model bias), consistently rule out a dynamic disorder of the H sites, confirming the occurrence of a static disorder in the structure of berborite-2*T*, at least at 20 K. Our X-ray data at 293 K cannot provide an unambiguous scenario for the H-bonding configuration at room temperature, a limitation also reported in all the previous X-ray studies (*e.g.*, Schlatti 1967, 1968; Giuseppetti et al. 1990; Aksenov et al. 2024). However, the best figure of merit of the structural model at 293 K shows the *H1* and *H2* atomic coordinates consistent to those refined from neutron data. This leads to a configuration in which the bonding parameters (*i.e.,* O_D-H, H…O_A, O_D…O_A, and O_D-H…O_A) do not show evidence of H-bonds involving potential mobile protons (by partial

proton transfer mechanisms from *donor* to *acceptor*) (Table 7), as previously observed in berborite-1*T* polytype by Aksenov et al. (2024). These findings leave open the question of whether different polytypes can have different proton behaviour at room temperature.

The effect of temperature on the crystal structure of berborite cannot be realistically disclosed in terms of the H-bonding network, as room-*T* X-ray data cannot provide a clear picture of H site location and libration. However, a comparative analysis of the structures refined at 293 K (X-ray) and 20 K (neutron) can be conducted based on the geometry of the BO_3- and $BeO_3\Phi$-units. The *B1-O1s* distance tends to increase with decreasing temperature ($\Delta l \sim 0.012$ Å, between 293 and 20 K) (Table 7); the same trend was also observed in the *in-situ* low-*T* X-ray diffraction experiments by Aksenov et al. (2024). The aplanarity of the BO_3-unit, here defined as the average angle described by the plane on which the 3-oxygen sites lie and each of the three independent B-O_n vectors, is ~2.6° at 293 K, and increases to ~9.5° at 20 K (Table 7); this reflects increasing deformation of the triangular unit at low temperature, in terms of out-of-plane displacement of the *B1* site. More complex is the temperature behaviour of the tetrahedral units: *i)* the two independent bond distances of the *BeA*-tetrahedron are indistinguishable at 293 K (*avg.* ~1.629 Å) and tend to shorten and differentiate at low temperature (with a difference of ~0.012 Å, *avg.* 1.617 Å at 20 K) (Table 7); *ii)* the two independent bond distances of the *BeB*-tetrahedron are similar at 293 K (with a difference of ~0.005 Å, *avg*. 1.630 Å) and increase significantly at low temperature (*avg*. 1.646 Å), though maintaining a modest difference in length (~0.004 Å) (Table 7). It is worth noting that, at low-*T*, neutron data reveals what is partially veiled at room-*T*, probably due to the high atomic libration: the Be-OH and Be-OH_2 bonds are significantly different, with *BeA-O2A* of ~1.626 Å and *BeB-O2B* of ~1.649 Å (Table 7). This difference is dictated by the fact that the oxygen *O2A* (of the hydroxyl group *O2A-H1*) is more strongly bonded to beryllium compared to *O2B* (of the molecule *H2-O2B-H2*), as *O2A* is comparatively less saturated than its counterpart. This is additional evidence of the different locations of the OH- and OH_2-groups in the structure of berborite-2*T*, making the *BeA*- and *BeB*-tetrahedra non-equivalent, in contrast to what was previously supposed by Schlatti (1967, 1968) for berborite-1*T*.

The combined behaviour of the BO_3- and $BeO_3\Phi$-units, and in particular the expansion of *B1-O1s* and *BeB-O1s* at low temperature, is also reflected by expansion of the unit cell on (0001) at 20 K, as also observed for berborite-1*T* by Aksenov et al. (2024), whereas along [0001] the uncertainty of our data obscures any potential trend (within 3σ) (Tables 3 and 7). The low-temperature experiment of Aksenov et al. (2024), based on X-ray data collected at 293, 240, 120, and 90 K, shows a non-

monotonic trend of the unit-cell volume with *T*: the volume appears first to decrease between 293 and 240 K, followed by an increase between 240 and 90 K. In this light, it is not surprising that the unit-cell volume measured by neutron data at 20 K (*i.e.,* 181.93(6) $Å^3$) is slightly larger than that measured by X-ray data at 293 K (*i.e.,* 181.390(9) $Å^3$, Table 3), and mainly arises due to expansion of the unit cell on (0001) at low temperature.

A material that shows some structural similarities with berborite is hambergite ($Be_2BO_3(OH,F)$). The structure of hambergite, reinvestigated by single-crystal neutron Laue diffraction by Gatta et al. (2012), is described in the space group *Pbca*, with $a \sim 9.762$, $b \sim 12.201$, and $c \sim 4.430$ Å, and made by the following building units: two independent $BeO_3(OH)$ tetrahedra and one BO_3 triangular unit. The unique OH-group is shared between the two independent $BeO_3(OH)$ tetrahedra, such that each non-hydroxyl oxygen site of the $BeO_3(OH)$ tetrahedra is shared with another $BeO_3(OH)$- or a BO_3-unit. This inter-polyhedral connection generates a framework-like structure (see Fig. 1 in Gatta et al. 2012). The refined H-bonding scheme in the crystalline edifice of hambergite is comparatively simple: one *donor* site and one *acceptor* site, having O_D-H~0.993 Å, $O_D...O_A \sim 2.904$ Å, $H...O_A \sim 1.983$ Å, and O_D-$H...O_A \sim 157.5°$. A zigzag chain of H-bonds along [001] occurs in the structure of hambergite. No evidence of disorder, pertaining to the H site, was reported by Gatta et al. (2012). Despite some similarities in terms of building-block units, the structures of hambergite and berborite are profoundly different. This is mainly generated by the OH-group and H_2O molecule bonded to the two independent Be sites, as apical (and unshared) vertices of tetrahedra in the structure of berborite, whereas in hambergite the OH-group acts as a bridging site between two tetrahedra.

This study, along with the previous investigation of hambergite, provides a picture about how single-crystal neutron diffraction can be successfully used in mineralogy in order to: *i*) locate light elements (in particular hydrogen, lithium, boron and beryllium), as neutrons interact with the atomic nuclei (and not with the electron cloud of atoms, as X-rays do), making neutrons sensitive to all elements, including the low-*Z* ones, and *ii*) yield a better description of atomic displacement around equilibrium positions, as neutron scattering power does not fall off with angle (as X-rays do), making possible measurements at high values of $\sin\theta/\lambda$ (required for a better definition of the atomic displacement).

Acknowledgements

The authors thank the Institut Laue-Langevin (Grenoble, France) for the allocation of the beamtime (DOI: 10.5291/ILL-DATA.5-11-458). X-ray (with KUMA diffract.) and EPMA-WDS data were collected using the facilities of the UniTech COSPECT - University of Milan (Italy). GDG and NR acknowledge the support of the Italian Ministry of Education (MUR) through the projects 'Dipartimenti di Eccellenza 2023-2027'. The Associate Editor, A. dos Santos, two anonymous Reviewers and the Technical Editor are warmly thanked for the revision of the manuscript.

References

Aksenov, S.M., Chukanov, N.V., Tarasov, V.P., Banaru, D.A., Mackley, S.A., Banaru, A.M., Krivovichev, S.V., and Burns, P.C. (2024) The local state of hydrogen atoms and proton transfer in the crystal structure of natural berborite, $Be_2(BO_3)(OH)\cdot H_2O$: Low-temperature single crystal X-ray analysis, IR and ^1H NMR spectroscopy, and crystal chemistry and structural complexity of beryllium borates. Journal of Physics and Chemistry of Solids, 189C, 111944.

Archer, J. and Lehmann, M.S. (1986) A simple adjustable mount for a two-stage cryorefrigerator on an Eulerian cradle. Journal of Applied Crystallography, 19, 456-459.

Busing, W.R. and Levy, H.A. (1964) The effect of thermal motion on the estimation of bond lengths from diffraction measurements. Acta Crystallographica, 17, 142-146.

Chiari, G. and Ferraris, G. (1982) The water molecules in crystalline hydrates studied by neutron diffraction. Acta Crystallographica, B38, 2331–2341.

Collins D.M. (1982) Electron density images from imperfect data by iterative entropy maximization. Nature, 298, 49–51.

Dyar, M.D., Wiedenbeck, M., Robertson, D., Cross, LR., Delaney, J.S., Ferguson, K., Francis, C.A., Grew, E.S., Guidotti, C.V., Hervig, R.L., Hughes, J.M., Husler, J., Leeman, W., McGuire, A.V., Rhede, D., Rothe, H., Paul, R.L., Richards, I., and Yates, M. (2001) Reference Minerals for the Microanalysis of Light Elements. Geostandards Newsletter, 25, 441.463.

Fleischer M. (1968) New mineral names. American Mineralogist, 53, 348-351.

Gatta, G.D., Rotiroti, N., McIntyre, G.J., Guastoni, A., and Nestola, F. (2008) New insights into the crystal chemistry of epididymite and eudidymite from Malosa, Malawi: a single-crystal neutron diffraction study. American Mineralogist, 93, 1158-1165.

Gatta, G.D., McIntyre, G.J., Bromiley, G., Guastoni, A., and Nestola, F. (2012) A single-crystal neutron diffraction study of hambergite, $Be_2BO_3(OH,F)$. American Mineralogist, 97, 1891–1897.

Gatta, G.D., Hradil, K., and Meven, M. (2021) Where is the Hydrogen? Elements, 17, 163-168.

Gatta, G.D., Cannaò, E., Comboni, D., Battiston ,T., and Fabelo, O. (2024) A neutron diffraction study of the hydrous borate inderborite, $CaMg[B_3O_3(OH)_5]_2(H_2O)_4 \cdot 2H_2O$. American Mineralogist, 109, 1258-1265

Giuseppetti, G., Mazzi, F., Tadini, C., Larsen, A.O., Asheim, A., and Raade, G. (1990) Berborite polytypes. Neues Jahrbuch für Mineralogie – Abhandlungen, 162, 101–116.

Larsen A.O. (2010) The Langesundsfjord. History, geology, pegmatites, minerals. Bode Verlag GmbH, Salzhemmendorf (Germany), 239 pages, ISBN 978-3-925094-97-2.

Larson A.C. (1967) Inclusion of secondary extinction in least-squares calculations. Acta Crystallographica, 23, 664-665.

Momma, K., Ikeda, T., Belik A.A., and Izumi, F. (2013) Dysnomia, a computer program for maximum-entropy method (MEM) analysis and its performance in the MEM-based pattern fitting. Powder Diffraction, 28, 184-193.

Nefedov E.I. (1967) Berborite, a new mineral. Doklady Akademii Nauk SSSR, 174, 189-192.

Nefedov, E.I., Griffin, W.L., and Kristiansen, R. (1977) Minerals of the schoenfliesite-wickmanite series from Pitkliranta, Karelia, U.S.S.R. Canadian Mineralogist, 15, 437-445.

Nikolskaya Z.D., Larin A.M. (1972) Greisen formation of the Pitkäranta ore field. Zapiski Vsesoyuznogo Mineralogicheskogo Obshchestva 101, 290-297.

Rigaku Oxford Diffraction (2019) *CrysAlisPro* Software system, version 1.171.40.67a, Rigaku Corporation, Wroclaw (Poland).

Schlatti M. (1967) Synthese und Strukturtyp des Berylliumborates $Be_2BO_3(OH)H_2O$. Naturwissenschaften, 54, 587-587.

Schlatti, M. (1968) Hydrothermalsynthese und Strukturtyp des Berylliumborates $Be_2BO_3OH.H_2O$. Tschermaks Mineralogische und Petrographische Mitteilungen, 12, 463–469.

Sears, V.F. (1986) Neutron Scattering Lengths and Cross-Sections. In K. Sköld and D.L. Price, Eds., Neutron Scattering, Methods of Experimental Physics, Vol. 23A, Academic Press, New York, pp. 521-550.

Sheldrick, G.M. (2015) Crystal structure refinement with SHELXL. Acta Crystallographica Section C: Structural Chemistry, 71, 3-8.

Steiner, T. (1998) Opening and narrowing of the water H-O-H angle by hydrogen-bonding effects: Re-inspection of neutron diffraction data. Acta Crystallographica, B54, 464–470.

Wilkinson, C., Khamis, H.W., Stansfield, R.F.D., and McIntyre, G.J. (1988) Integration of single-crystal reflections using area multidetectors. Journal of Applied Crystallography, 21, 471-478.

This is the peer-reviewed, final accepted version for American Mineralogist, published by the Mineralogical Society of America.
The published version is subject to change. Cite as Authors (Year) Title. American Mineralogist, in press.
DOI: https://doi.org/10.2138/am-2025-10029. http://www.minsocam.org/

Tables

Table 1. Concentration (wt%) of a series of elements measured by EPMA-WDS (10 data points) in berborite.

Element/Oxide	***Min-Max***	***Avg.***
Na_2O	*b.d.l.* - 0.0522	0.0128
K_2O	*b.d.l.* - 0.0154	0.0026
CaO	0.0063 - 0.1238	0.0603
MgO	*b.d.l.* - 0.0319	0.0089
FeO	*b.d.l.* - 0.0277	0.0076
SO_3	*b.d.l.* - 0.0387	0.0065
F	*b.d.l.*	*b.d.l.*
Cl	*b.d.l.*	*b.d.l.*

b.d.l. = below the detection limit

Table 2. Raw SIMS data for hambergite #102984 (used as standard) and berborite.

Sample	**$^{1}H/^{9}Be$**	**$^{11}B/^{9}Be$**	**^{9}Be cps**	**$^{7}Li/^{9}Be$**	**$^{19}F/^{9}Be$**	**$^{27}Al/^{9}Be$**	**$^{28}Si/^{9}Be$**	**$^{35}Cl/^{9}Be$**
hambergite_1	0.0220(9)	0.1633(2)	1.156E+06	0	7.79E-05	1.28E-05	1.68E-06	0
hambergite_2	0.0217(7)	0.1632(2)	1.173E+06	0	7.87E-05	1.28E-05	2.13E-06	0
average	**0.0219(2)**	**0.1633(2)**	**1.165E+06**		**7.83E-05**	**1.28E-05**	**1.90E-06**	
berborite_1	0.04208(3)	0.1634(3)	1.182E+06	2.15E-07	6.61E-06	2.66E-05	3.62E-03	0
berborite_2	0.04186(10)	0.1632(2)	1.204E+06	7.01E-08	4.13E-06	7.73E-06	4.76E-03	2.06E-08
berborite_3	0.04134(13)	0.1632(1)	1.200E+06	1.77E-07	7.52E-06	7.47E-06	4.31E-03	2.13E-08
berborite_4	0.04152(8)	0.1631(2)	1.210E+06	7.03E-08	9.04E-06	8.83E-06	4.84E-03	0
berborite_5	0.04249(8)	0.1624(2)	1.204E+06	0	3.91E-06	1.11E-05	5.35E-03	2.07E-08
berborite_6	0.04188(6)	0.1637(2)	1.176E+06	7.15E-08	6.38E-06	1.47E-05	2.27E-03	0
average	**0.04186(41)**	**0.1632(4)**	**1.196E+06**	**1.01E-07**	**6.26E-06**	**1.27E-05**	**4.19E-03**	

Standard deviations for $^{1}H/^{9}Be$ and $^{11}B/^{9}Be$ are indicated by variation in the last digit(s) between parentheses.

This is the peer-reviewed, final accepted version for American Mineralogist, published by the Mineralogical Society of America.
The published version is subject to change. Cite as Authors (Year) Title. American Mineralogist, in press.
DOI: https://doi.org/10.2138/am-2025-10029. http://www.minsocam.org/

Table 3 (*deposited*). Details of X-ray and neutron data collections and refinements of berborite.

	Neutron	**X-ray**
T (K)	20(1)	293(1)
Crystal shape	Di-trigonal pyramid	Prism
Crystal size (mm)	2.2 x 2.2 x 3.1	0.08 × 0.12 × 0.18
Crystal colour	Colourless, white	Colourless, white
Unit-cell parameters	a = 4.4389(7) Å	a = 4.4319(1) Å
	c = 10.662(1) Å	c = 10.6636(2) Å
	V = 181.93(6) Å^3	V = 181.390(9) Å^3
Reference chemical formula	$Be_2(BO_3)(OH)\cdot H_2O$	$Be_2(BO_3)(OH)\cdot H_2O$
Space Group	$P3c1$	$P3c1$
Z	1	1
Radiation type, λ (Å)	Neutron CW, 0.835	X-ray, Mo-$K\alpha$
Diffractometer	D9 four-circle - ILL	Rigaku XtaLABSynergy-i
Data-collection method	ω-scans (low-Q), ω-2θ-scans (high-Q)	ω-scan
$d_{min.}$ (Å)	0.50	0.58
	$-8 \le h \le +8$	$-7 \le h \le +7$
	$-9 \le k \le +8$	$-7 \le k \le +7$
	$-19 \le l \le +3$	$-18 \le l \le +17$
Measured reflections	2130	14472
Unique reflections	356	628
Unique reflections with $F_o > 4\sigma(F_o)$	350	625
Extinction coefficient	0.40(4)	0.49(5)
Refined parameters	43	33
R_{Int}(Laue class $\bar{3}m$)	0.0320	0.0332
R_σ	0.0200	0.0096
R_1 *(F)* with $F_o > 4\sigma(F_o)$	0.0358	0.0264
R_1 *(F)* for all reflections	0.0363	0.0264
$wR_2(F^2)$	0.0923	0.0662
GooF	1.183	1.122
Residuals (fm/Å^3, e-/Å^3)	-1.2/+1.5	-0.25/+0.39

Note: Statistical parameters according to the SHELXL-2018/3 definition.

This is the peer-reviewed, final accepted version for American Mineralogist, published by the Mineralogical Society of America.
The published version is subject to change. Cite as Authors (Year) Title. American Mineralogist, in press.
DOI: https://doi.org/10.2138/am-2025-10029. http://www.minsocam.org/

Table 4 (*deposited*). Refined fractional atomic coordinates and equivalent/isotropic displacement parameters (Å^2) of berborite, based on the neutron structure refinement (data collected at 20 K) and X-ray refinement (data collected at 293 K). U_{eq} is defined as one third of the trace of the orthogonalised U_{ij} tensor; *s.o.f.* = site occupancy factor.

		Neutron ref.					***X-ray ref.***				
Site	*Element*	*s.o.f.*	*x/a*	*y/b*	*z/c*	U_{eq}	*s.o.f.*	*x/a*	*y/b*	*z/c*	U_{eq}/U_{iso}
BeA	Be	1.0	2/3	1/3	0.3035(2)	0.0126(6)	1.0	2/3	1/3	0.2899(3)	0.0074(4)
BeB	Be	1.0	1/3	2/3	0.2002(2)	0.0091(5)	1.0	1/3	2/3	0.1876(4)	0.0095(2)
B1	B	1.0	0	0	0.2424(6)	0.0092(5)	1.0	0	0	0.2361(5)	0.0074(2)
O1	O	0.131(7)	-0.325(3)	-0.023(5)	0.252(2)	0.0124(3)	0	/	/	/	/
O1s	O	0.869(7)	-0.0034(8)	0.3085(5)	0.2532(6)	0.0124(3)	1.0	0.0007(7)	0.3093(4)	0.2390(3)	0.0090(2)
O2A	O	1.0	2/3	1/3	0.4560(5)	0.0244(11)	1.0	2/3	1/3	0.4426(1)	0.0188(4)
O2B	O	1.0	1/3	2/3	0.0456(4)	0.0157(9)	1.0	1/3	2/3	0.0346(1)	0.0198(5)
H1	H	1/3	0.891(6)	0.449(6)	0.490(2)	0.0340(11)	1/3	0.88(2)	0.50(2)	0.469(9)	0.024(8)
H2	H	2/3	0.078(3)	0.539(3)	0.0063(10)	0.0340(11)	2/3	0.109(11)	0.531(11)	-0.002(5)	0.024(8)

s.o.f.(*O1*)+*s.o.f.*(*O1s*)=1.0

Table 5 (*deposited*). Refined displacement parameters (Å^2) of berborite, as described in the expression: $-2\pi^2[(ha^*)^2U_{11} + \ldots + 2hka^*b^*U_{12} + \ldots + 2klb^*c^*U_{23}]$, based on the neutron structure refinement (at 20 K) and on the X-ray refinement (at 293 K).

Neutron	U_{11}	U_{22}	U_{33}	U_{23}	U_{13}	U_{12}
BeA	0.0142(8)	0.0142(8)	0.0095(9)	0	0	0.0071(4)
BeB	0.0054(6)	0.0054(6)	0.0164(10)	0	0	0.0027(3)
B1	0.0085(6)	0.0085(6)	0.0106(14)	0	0	0.0043(3)
O1	0.0095(6)	0.0105(9)	0.0167(6)	0.0043(11)	0.0008(4)	0.0047(8)
O1s	0.0095(6)	0.0105(9)	0.0167(6)	0.0043(11)	0.0008(4)	0.0047(8)
O2A	0.0285(18)	0.0285(18)	0.0163(17)	0	0	0.0143(9)
O2B	0.0186(14)	0.0186(14)	0.0098(14)	0	0	0.0093(7)
H1	0.034(2)	0.038(2)	0.0268(16)	0.000(2)	-0.0008(19)	0.015(2)
H2	0.034(2)	0.038(2)	0.0268(16)	0.000(2)	-0.0008(19)	0.015(2)

$U_{ij}(O1)=U_{ij}(O1s)$, $U_{ij}(H1)=U_{ij}(H2)$

X-ray	U_{11}	U_{22}	U_{33}	U_{23}	U_{13}	U_{12}
BeA	0.0068(5)	0.0068(5)	0.0085(7)	0	0	0.0034(2)
BeB	0.0059(2)	0.0059(2)	0.0166(3)	0	0	0.0030(1)
B1	0.0047(3)	0.0047(3)	0.0128(5)	0	0	0.0024(1)
O1s	0.0055(2)	0.0056(2)	0.0170(2)	-0.00002(14)	0.0007(1)	0.0036(2)
O2A	0.0236(6)	0.0236(6)	0.0090(6)	0	0	0.0118(3)
O2B	0.0228(6)	0.0228(6)	0.0139(7)	0	0	0.0114(3)

This is the peer-reviewed, final accepted version for American Mineralogist, published by the Mineralogical Society of America.
The published version is subject to change. Cite as Authors (Year) Title. American Mineralogist, in press.
DOI: https://doi.org/10.2138/am-2025-10029. http://www.minsocam.org/

Table 6 (*deposited*). Principal root-mean-square components (Å) of the atomic displacement parameters, based on the neutron structure refinement (data collected at 20 K) and X-ray refinement (data collected at 293 K).

Neutron	RMS_{min}	RMS_{mid}	RMS_{max}	RMS_{max}/RMS_{min}
BeA	0.0973	0.1190	0.1190	1.224
BeB	0.0738	0.0738	0.1280	1.736
B1	0.0923	0.0923	0.1032	1.118
O1	0.0909	0.0980	0.1386	1.525
O1s	0.0909	0.0980	0.1386	1.525
O2A	0.1275	0.1688	0.1688	1.324
O2B	0.0992	0.1365	0.1365	1.376
H1	0.1634	0.1834	0.2044	1.251
H2	0.1634	0.1834	0.2044	1.251

E.s.d. of *RMSs* on the last digit. *RMSs*(*O1*)=*RMSs*(*O1s*), *RMSs*(*H1*)=*RMSs*(*H2*)

X-ray	RMS_{min}	RMS_{mid}	RMS_{max}	RMS_{max}/RMS_{min}
BeA	0.0827	0.0827	0.0923	1.116
BeB	0.0770	0.0770	0.1288	1.673
B1	0.0686	0.0686	0.1130	1.647
O1s	0.0629	0.0781	0.1305	2.075
O2A	0.0951	0.1537	0.1538	1.618
O2B	0.1179	0.1509	0.1509	1.280

E.s.d. of *RMSs* on the last digit.

This is the peer-reviewed, final accepted version for American Mineralogist, published by the Mineralogical Society of America.
The published version is subject to change. Cite as Authors (Year) Title. American Mineralogist, in press.
DOI: https://doi.org/10.2138/am-2025-10029. http://www.minsocam.org/

Table 7. Relevant bond distances (Å) and angles (°) based on the neutron structure refinement (at 20 K) and the X-ray refinement (at 293 K) of berborite.

	Neutron	***X-ray***
B1-O1s (x 3)	1.382(2)	1.3696(5)
BeA-O1s (x 3)	1.614(4)	1.629(3)
BeA-O2A	1.626(6)	1.628(4)
BeB-O1s (x 3)	1.645(3)	1.627(3)
BeB-O2B	1.649(5)	1.632(4)
O1s-B1-O1s (x 3)	119.31(9)	119.95(1)
APL	9.5(1)	2.6(1)
O1s-BeA-O1s (x 3)	109.5(2)	109.5(2)
O1s-BeA-O2A (x 3)	109.4(2)	109.5(2)
O1s-BeB-O1s (x 3)	108.8(2)	109.3(2)
O1s-BeB-O2B (x 3)	110.1(2)	109.7(2)
O2A-H1 (x 3)	0.936(22)	0.91(9)
*O2A-H1**	0.998	/
O2A…O2B	2.735(2)	2.7406(6)
H1…O2B	1.801(23)	1.89(8)
O2A-H1…O2B	175.6(25)	155(8)
O2B-H2 (x 3)	1.067(11)	0.95(4)
*O2B-H2**	1.113	/
O2B…O2A	2.735(2)	2.7406(6)
H2…O2A	1.670(11)	1.80(4)
O2B-H2…O2A	175.7(12)	169(4)
H2-O2B-H2	105.6(7)	104(2)
B1-O1 (x 3)	1.398(10)	
BeA-O1 (x 3)	1.69(2)	
BeB-O1 (x 3)	1.56(2)	
O1-B1-O1 (x 3)	119.4(3)	
O1-BeA-O1 (x 3)	110.1(7)	
O1-BeA-O2A (x 3)	108.8(7)	
O1-BeB-O1 (x 3)	108.0(8)	
O1-BeB-O2B (x 3)	110.9(7)	

* Bond distance corrected for "riding motion" effect, following Busing and Levy (1964).
APL is the aplanarity of the triangular BO_3-group, here calculated as the average angle (°) described by the plan on which the 3-oxygen sites lie and each of the three independent B-O_n vectors.

This is the peer-reviewed, final accepted version for American Mineralogist, published by the Mineralogical Society of America.
The published version is subject to change. Cite as Authors (Year) Title. American Mineralogist, in press.
DOI: https://doi.org/10.2138/am-2025-10029. http://www.minsocam.org/

Figures

Figure 1. (*Left side*) Polyhedral representation of the crystal structure of berborite by a clinographic view based on the neutron structure refinement of this study (data collected at 20 K), and (*right side*) configuration of the substructure made by the additional O1 sites with partial occupancy factors (see text for details). Displacement ellipsoid probability factor: 50%.

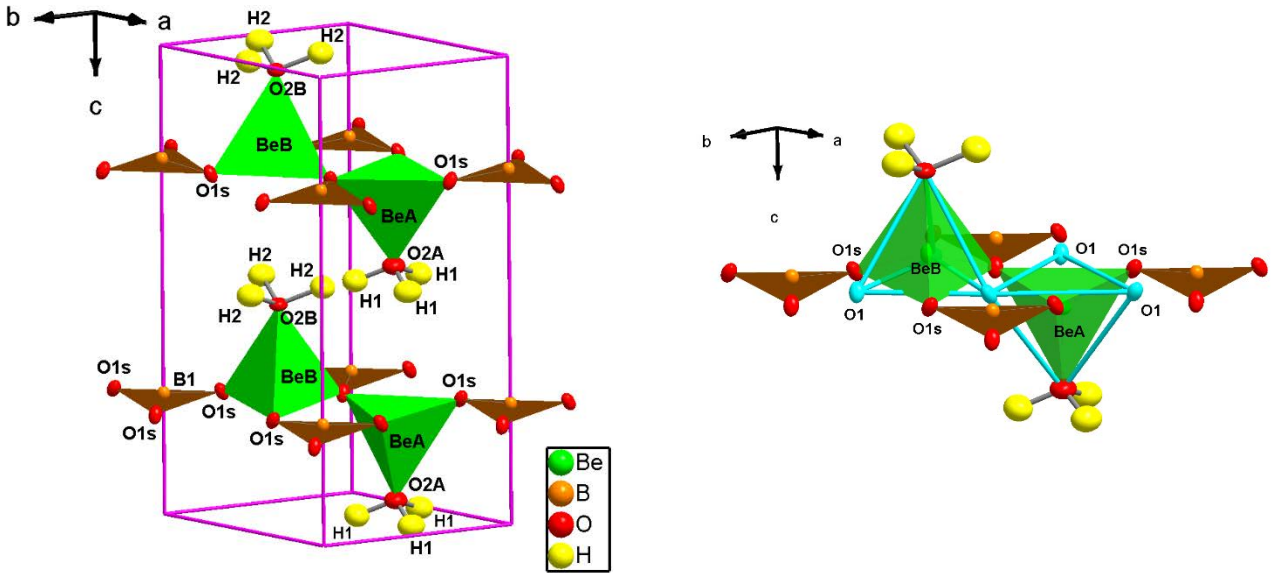

This is the peer-reviewed, final accepted version for American Mineralogist, published by the Mineralogical Society of America.
The published version is subject to change. Cite as Authors (Year) Title. American Mineralogist, in press.
DOI: https://doi.org/10.2138/am-2025-10029. http://www.minsocam.org/

Figure 2. (0001) section of the difference-Fourier map of the nuclear density function at z=1/2, phased without any H sites in the structural model. The symmetry-related positions of the *H1* and *H2* sites are clearly visible as minima of the map (because H has a negative neutron scattering length). The *H2* sites show higher nuclear density. Scale in fm/Å^3. Map orientation: $x \rightarrow$.

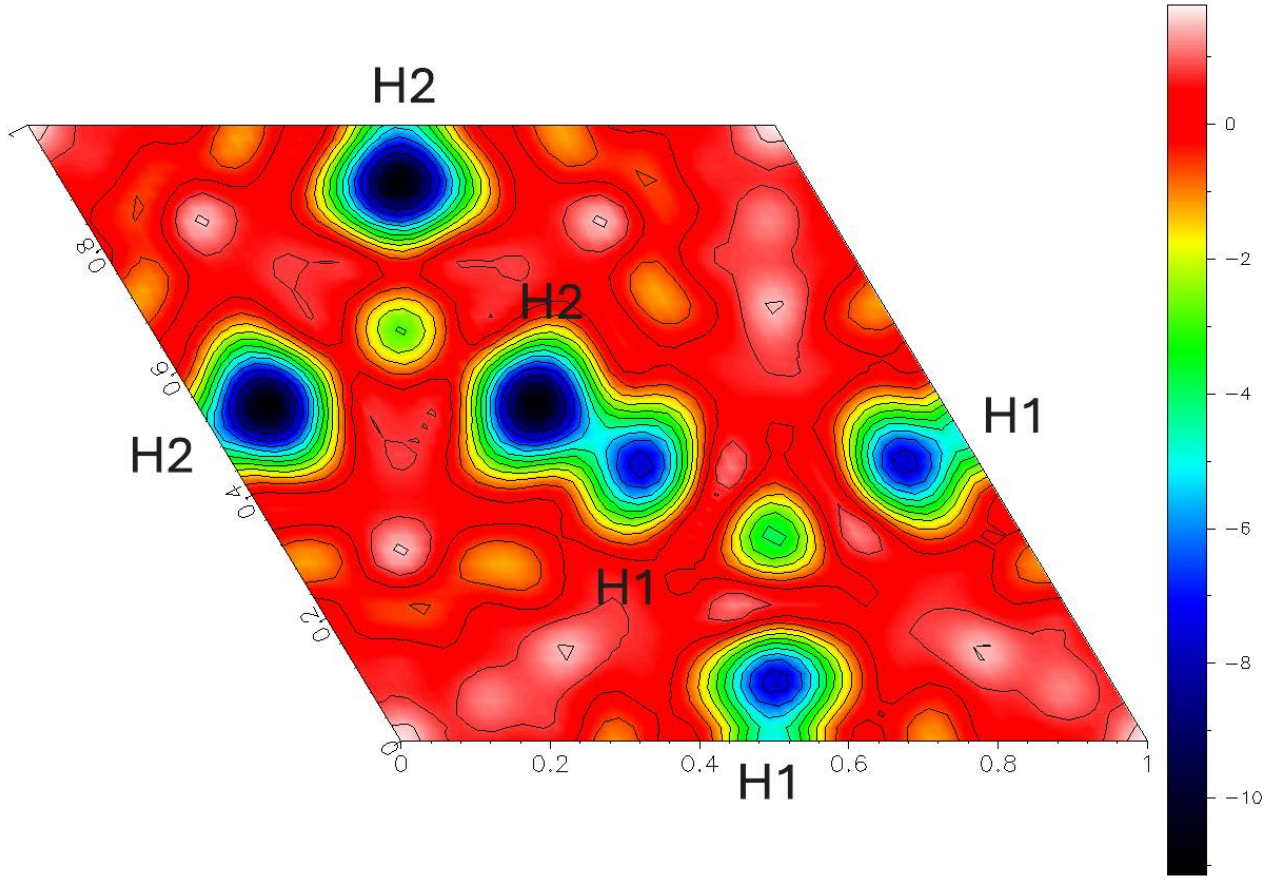

This is the peer-reviewed, final accepted version for American Mineralogist, published by the Mineralogical Society of America.
The published version is subject to change. Cite as Authors (Year) Title. American Mineralogist, in press.
DOI: https://doi.org/10.2138/am-2025-10029. http://www.minsocam.org/

763 Figure 3. MEM analysis: (0001) section the at z=1/2. The analysis was carried out using the *Dysnomia*
764 program (Momma et al. 2013), which implements MEM in conjunction with structure factor data
765 obtained from least-square single-crystal neutron diffraction refinement. The maximum entropy map
766 shows positive density around the positions of the O atoms, while negative density at the H positions.
767 Scale in fm/Å^3. Map orientation: $x \rightarrow$.

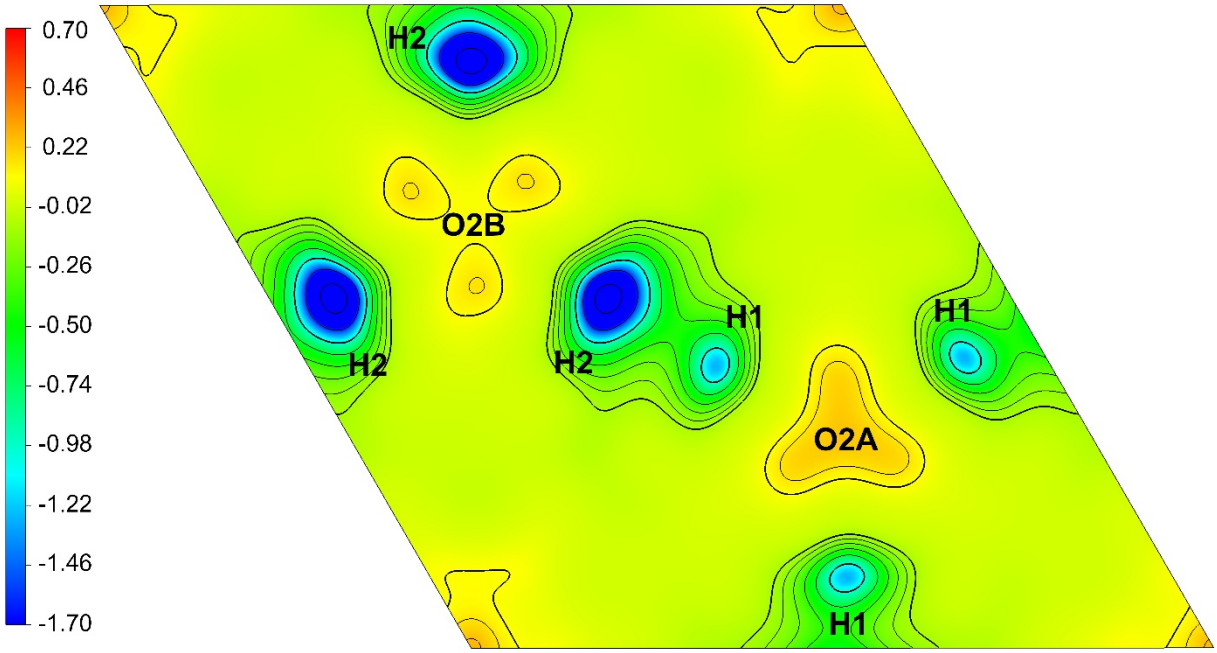

768

Figure 4. One of the potential H-bonding schemes within the structure of berborite, as dictated by disordered configuration of the H sites, based on the neutron structure refinement of this study. Displacement ellipsoid probability factor: 50%.